BEST AVAILABLE IMAGES

Defective images within this document are accurate representations of the original documents submitted by the applicant.

Defects in the images may include (but are not limited to):

- BLACK BORDERS
- TEXT CUT OFF AT TOP, BOTTOM OR SIDES
- FADED TEXT
- ILLEGIBLE TEXT
- SKEWED/SLANTED IMAGES
- COLORED PHOTOS
- BLACK OR VERY BLACK AND WHITE DARK PHOTOS
- GRAY SCALE DOCUMENTS

IMAGES ARE BEST AVAILABLE COPY.

As rescanning documents *will not* correct images, please do not report the images to the Image Problem Mailbox.

2096 Glastech[illegible]he Berichte
64(1991)Januar, No.1, Frankfurt, DE

Original Paper

Glass fiber dissolution in a physiological saline solution

Russell M. Potter and Stephanie M. Mattson

Owens-Corning Fiberglas Corporation, Technical Center Granville, Glass Research and Inorganic Analysis Laboratory, Granville, OH (USA)

A technique developed to measure the dissolution rate of glass fibers in the laboratory under conditions approximating those thought to exist in the lung has been applied to 30 glass compositions in the SiO_2–Al_2O_3–B_2O_3–CaO–MgO–BaO–Na_2O system. Dissolution rates show an Arrhenius dependence on temperature with an activation energy near 64 kJ/mol. The rate increases with the pH value. Glass fiber dissolution is a leaching process which leaves behind a mechanically-weak layer consisting of SiO_2 and Al_2O_3. Dissolution morphology changes with dissolution rate, suggesting a change in dissolution mechanism. Dissolution rates vary with composition from 0.9 to 887 ng/(cm² h). Al_2O_3 strongly decreases the dissolution rate, B_2O_3, BaO, CaO, MgO, and Na_2O increase the rate to about the same degree, and SiO_2 has little effect.

Auflösung von Glasfasern in einer physiologischen Salzlösung

In Anlehnung an Bedingungen, deren Vorliegen in der Lunge man annimmt, wurde ein Verfahren zur Auflösung von Glasfasern entwickelt und auf 30 Glaszusammensetzungen des Systems SiO_2–Al_2O_3–B_2O_3–CaO–MgO–BaO–Na_2O angewendet. Die Auflösungsgeschwindigkeiten zeigen eine Arrhenius-Abhängigkeit von der Temperatur mit einer Aktivierungsenergie von etwa 64 kJ/mol. Die Geschwindigkeit nimmt mit dem pH-Wert zu. Die Glasfaserauflösung ist ein Auslaugprozeß, der eine mechanisch instabile Schicht aus SiO_2 und Al_2O_3 zurückläßt. Die bei der Auflösung an der Glasoberfläche sich ausbildende Morphologie hängt von der Auflösungsgeschwindigkeit ab, was die Annahme nahelegt, daß sich der Auflösungsmechanismus ändert. Die Auflösungsgeschwindigkeiten variieren mit der Zusammensetzung von 0,9 bis 887 ng/(cm² h). Al_2O_3 reduziert die Auflösungsgeschwindigkeit deutlich, während B_2O_3, BaO, CaO, MgO und Na_2O diese in etwa gleichem Maße beschleunigen. SiO_2 zeigt nur einen geringen Einfluß.

1. Introduction

In recent years there has been increasing interest in the health effects of inhaled fibrous material. Asbestos fibers have been shown to cause cancer and other lung diseases, and there is concern that other fibrous materials may cause similar health problems as a result of their fibrous geometry. It has been hypothesized that the residence time of fibers in the lung has a strong influence on their ability to cause disease, and that this residence time depends strongly on the clearance rate and the dissolution rate of the fibrous material. For this reason, a number of studies have been conducted to measure the dissolution rates of various inorganic fibers under conditions thought to be similar to those in the lung [1 to 6]. These studies have surveyed many types of inorganic fibers. They suggest that the chemical composition of fibers can have a strong influence on the dissolution rate, but variations in the physical characteristics of the sample limit their usefulness in understanding the relation between chemical composition and dissolution rate. Nor has there been any detailed study of the dissolution mechanism. This report presents the results of a systematic study of glass fiber dissolution rate and mechanism for glasses in the SiO_2–Al_2O_3–B_2O_3–CaO–MgO–BaO–Na_2O system using glass fiber samples melted and formed in the laboratory to approximately the same uniform diameter.

Received 5 June 1990.

2. Experimental procedure and rationale

Glasses were prepared from reagent grade materials by melting in a covered Pt-Rh alloy crucible for 3 h at 1450 °C in an electric furnace. After each hour, the melt was removed from the furnace and stirred briefly to improve glass homogeneity. Fibers of uniform diameter were formed by standard techniques from a one-hole Pt-Rh alloy bushing. The fibers were cut into approximately 1 cm lengths and stored in sealed plastic containers in a desiccator.

Fiber diameter measurements were made on polished cross sections of expoxy-embedded fibers using a Scanning Electron Microscope (SEM). The number of measurements made for each sample was generally in the range 20 to 50. Fibers near 10 µm in diameter were routinely used in the experiments due to ease of formation and handling, but for four compositions; fibers near 2 µm in diameter were also formed to apply the dissolution technique to fibers of respirable diameter and to confirm that the dissolution-rate constant measured by this technique is a fundamental glass parameter independent of fiber geometry.

Fiber dissolution has generally been measured by monitoring either fiber weight loss or the dissolution fluid composition. Neither method is ideal. The dissolution process at physiological pH values involves both selective leaching and network dissolution. Fiber weight loss measurements do not allow distinguishing these two processes; complete analysis of the fluid for dissolved components is difficult or impossible because some are already present in the fluid in concentrations far exceeding the amounts dissolved. Neither method addresses morphological changes, which may lead to physical breakup of the fibers. As Scholze [5] points out in a general review of the fiber dissolution literature, it is clearly desirable to monitor all possible changes: solution composition, weight loss, chemical composition, and morphology of the fiber. For the present study, which aims at a general understanding of the effects of glass composition on dissolution, fiber weight loss data on many fiber compositions are sufficient to determine the basic compositional dependence. For some samples solution composition and changes in fiber morphology were also measured in addition to weight loss.

To prepare a sample for dissolution rate measurement, approximately 1.5 g of fiber was dispersed in deionized water by a 15 s treatment in a blender. The suspension was filtered through a 0.4 µm polycarbonate membrane filter backed by a plastic filter support pad in the bottom of a 37 mm diameter, three-section air-monitoring cassette. The cassette was reassembled, enclosing the sample between two 0.4 µm polycarbonate filters. The mat of fibers generally filled the 6.6 cm^3 space between the two filters. This procedure eliminates fiber bundles that could trap or exclude solution and locally alter the dissolution process. It allows the initial sample weight to be determined by difference from the preweighed cassette and filters. And it keeps the fibers enclosed throughout subsequent procedures. After filtration, the cassette was dried for 2 d under vacuum at 50 °C and then to constant weight in a glove box with $CaSO_4$ desiccant at room temperature. After final weighing, the sample was removed from the cassette and stored in a sealed plastic bag until needed for morphological studies.

The composition of the fluid-contacting fibers in the lung is not known although some constraints can be put on it [7]. Most of the simulated lung fluid compositions that have been used in the literature are based on the composition of interstitial fluid as reported by Gamble [8]. That used in this study is a modification of Gamble's solution developed by Kanapilly [9], in which the calcium concentration has been reduced to avoid precipitation of calcium salts (table 1). To eliminate bacterial and algal growth, 0.1 % NaN_3 has been added to this solution. Several experiments were run in different fluids to give some indication of the effect of solution composition.

Table 1. Physiological saline solution compositions in mg/l of solution and dissolution-rate constants for selected glasses

	modified from [9]	modified from [4]	modified human blood plasma[1])
Ca^{2+}	7.9	69.6	95
K^+	–	–	166
Mg^{2+}	–	21.3	25
Na^+	3363.3	3516.8	4267
NH_4^+	180.4	–	1
Cl^-	4481.4	4085.0	3651
HCO_3^-	1647.3	1963.3	1216
PO_4^{3-}	114.2	87.9	287
SO_4^{2-}	48.0	53.4	32
N_3^-	64.6	64.6	–
citrate	37.9	119.6	3171
glycine	450.0	118.0	–
tartrate	–	115.8	–
lactate	–	139.1	107
pyruvate	–	136.1	–
dextrin	–	–	3600
total protein	(450.0)	(118.0)	(> 72000)
k in ng/(cm^2 h)			
glass no. 5	27.4	51.6	25.4
glass no. 22	254.6	–	144.1

[1]) Outdated plasma from the American Red Cross, which has the following additives to whole blood: 3.7 g/l sodium citrate, 3.6 g/l dextrin, 460 mg/l citric acid, and 310 mg/l NaH_2PO_4. This plasma composition is based on typical values of human whole blood, plasma, or serum [10] with these additives.

Except for blood plasma and some solutions used in variable pH studies, the fluids were bubbled with a 5 % CO_2 in air mixture to maintain the pH value at 7.4.

For dissolution-rate measurements, the cassettes were placed into a water bath at 37.0 °C ± 0.5 K, and fluid was pumped through them at a rate of (0.20 ± 0.04) ml/min by peristaltic pumps. To avoid leakage, it was necessary to tap the cassettes for threaded fittings and to clamp the cassettes together. Except for short sections in the pumps, all tubing was TFE (teflon) to avoid gas diffusion through the tubing. For selected samples, the fluid pH value was monitored by flow-through pH electrodes both before and after the cassettes. The solution pH value prior to the cassettes was 7.4 ± 0.2. Solution pH after it had passed through the cassettes was initially between 8 and 9, but for most samples it dropped to 7.4 ± 0.2 within several hours. With the most rapidly dissolving samples it remained in the range 7.6 to 7.9 for the rest of the experiment. This observation indicates that the flow rate used in this study may have been too low for the rapidly dissolving glasses and that for these glasses, dissolution rate may change if flow rates were incr ased. Further tests will be run to determine if this problem existed and its effect, if any, on the measured fiber dissolution rate.

The durations of th experiments were generally 1, 2, 3, and 4 weeks. Individual samples were used for

Table 2. Calculated glass fiber oxide compositions[2]) in wt%

glass no.	SiO_2	Al_2O_3	CaO	MgO	Na_2O	K_2O	B_2O_3	TiO_2	Fe_2O_3	SrO	BaO	F_2
1	61.32	8.06	9.18	4.33	15.31	0.80	0.50	0.10	0.30	–	–	–
2	54.00	9.90	15.80	5.60	9.20	1.20	4.30	–	–	–	–	–
3	62.00	8.00	8.00	4.00	16.00	–	2.00	–	–	–	–	–
4	58.00	8.00	8.00	4.00	16.00	–	6.00	–	–	–	–	–
5	63.10	5.50	6.00	3.10	14.80	1.10	5.40	–	0.10	–	–	0.70
6	66.00	4.00	8.00	4.00	16.00	–	2.00	–	–	–	–	–
7	64.15	3.71	7.98	3.63	15.28	0.75	4.43	0.19	0.30	0.08	–	–
8	61.64	4.00	7.72	3.72	14.85	0.84	3.60	0.27	0.32	0.09	2.40	–
9	59.51	4.98	7.36	3.64	14.22	2.10	7.53	0.07	0.37	0.06	–	–
10	59.37	5.14	7.98	3.82	14.29	2.17	6.61	0.08	0.37	0.04	–	–
11	62.00	4.00	8.00	2.00	18.00	–	6.00	–	–	–	–	–
12	62.00	4.00	8.00	8.00	12.00	–	6.00	–	–	–	–	–
13	62.00	4.00	8.00	4.00	16.00	–	6.00	–	–	–	–	–
14	59.20	4.50	15.30	5.60	10.90	0.60	3.90	–	–	–	–	–
15	60.72	3.81	7.92	3.65	14.78	0.93	5.07	0.13	0.26	0.04	2.02	–
16	62.00	4.00	10.00	2.00	16.00	–	6.00	–	–	–	–	–
17	60.50	3.60	15.90	3.60	10.50	0.30	5.60	–	–	–	–	–
18a	61.99	3.93	7.91	3.50	14.63	0.77	6.97	0.05	0.17	0.08	–	–
18b	61.99	3.93	7.91	3.50	14.63	0.77	6.97	0.05	0.17	0.08	–	–
18c	61.99	3.93	7.91	3.50	14.63	0.77	6.97	0.05	0.17	0.08	–	–
19	62.00	4.00	4.00	8.00	16.00	–	6.00	–	–	–	–	–
20	60.16	3.66	8.09	3.14	14.42	0.91	6.04	0.19	0.25	0.12	2.45	–
21	62.00	4.00	12.00	4.00	12.00	–	6.00	–	–	–	–	–
22	62.00	4.00	6.00	4.00	18.00	–	6.00	–	–	–	–	–
23	64.71	2.10	8.60	3.60	14.90	0.43	5.40	0.07	0.12	0.02	–	–
24	60.00	4.00	8.00	4.00	16.00	–	8.00	–	–	–	–	–
25	59.39	3.36	7.97	3.59	14.23	0.60	9.78	0.34	0.32	–	–	–
26	64.00	2.00	8.00	4.00	16.00	–	6.00	–	–	–	–	–
27	65.69	0.50	5.66	3.02	15.78	0.80	8.04	0.10	0.30	–	–	–
28	62.00	2.00	8.00	4.00	16.00	–	8.00	–	–	–	–	–
29	66.00	–	8.00	4.00	16.00	–	6.00	–	–	–	–	–
30	62.94	0.90	8.70	1.18	16.06	0.18	9.56	0.03	0.18	0.20	–	–

[2]) Glass compositions are calculated from the raw material compositions with no attempt to correct for volatilization during melting. Glasses no. 18a to c are batches of fiber made from the same bulk glass at different times.

each time. At the end of the allotted time, the sample was removed from the water bath, cooled to room temperature and washed by switching the pump fluid to deionized water for at least 2 h. The cassette was then disconnected from the pumping lines, the water removed by suction filtration, and the cassette dried to constant weight in the manner already described. For several samples the dissolution was monitored for times up to 20 weeks to assure that the standard 4 week experiments gave results representative of dissolution at longer times.

SEM analyses of the partially-dissolved samples were performed on ≈ 1 cm diameter cores taken vertically at the center of each sample through the entire thickness. The core was cut in half lengthwise and embedded in epoxy resin. It was then ground briefly on the face of the cut and polished with diamond paste. This gives a polished section perpendicular to many fibers.

Chemical analysis of dissolution fluid and glass fibers was done by inductively-coupled plasma arc spectroscopy (atomic absorption spectroscopy for potassium). Dissolution fluid samples were collected in 50 ml polyethylene bottles directly from the outflow tubing. They were immediately frozen and stored in the freezer until analyzed. Glass fibers were dissolved in a mixture of aqua regia and hydrofluoric acid in a microwave oven prior to analysis of all elements but boron. For boron analysis the boron was brought into solution by leaching the fibers in hydrofluoric acid.

3. Dissolution rate constant calculation

Glass fiber dissolution rates were calculated from weight-loss data assuming that the rate is proportional to the reaction-surface area:

$$-\mathrm{d}M/\mathrm{d}t = kA \tag{1}$$

where M = fiber mass in ng at time t, t = time in h, k = dissolution-rate constant in ng/(cm^2 h), A = reaction-surface area in cm^2.

If the distribution of fiber diameters in the sample is assumed to be Gaussian, the following relation can be derived (section 8.1.):

$$\frac{M}{M_0} = \frac{b\exp(-b^2) + (\sqrt{\pi}/2)(1+2b^2)(1+\mathrm{erf}\,b)}{b_0\exp(-b_0^2) + (\sqrt{\pi}/2)(1+2b_0^2)(1+\mathrm{erf}\,b_0)} \tag{2}$$

Table 3. Glass fiber physical properties

glass no.	density[3]) in g/cm³	fiber diameter in µm	σ in µm	k in ng/(cm² h)	σ in ng/(cm² h)	type of morphology (see text)
1	2.52	8.85	0.84	0.9	0.2	–
2	2.59	9.40	0.30	3.0	0.5	–
3	2.50	8.92	0.31	5.4	1.4	–
4	2.52	9.39	0.33	9.0	2.1	–
5	2.51	9.62	0.45	27.4	1.1	A
6	2.49	9.41	0.39	42.7	3.4	–
7	2.51	8.21	0.32	49.2	4.4	–
8	2.57	9.48	1.50	57.5	2.5	–
9	2.51	8.88	1.02	77.7	6.8	A
10	2.52	9.15	0.97	84.1	11.3	–
11	2.53	9.25	0.24	108.0	4.8	A
12	2.52	8.84	0.42	109.9	11.9	A
13	2.51	9.97	0.32	139.0	4.8	A
14	2.59	9.21	0.39	142.9	12.3	–
15	2.56	9.27	0.99	150.1	20.6	–
16	2.53	9.24	0.28	166.6	11.5	A
17	2.59	9.56	0.33	202.2	1.6	A
18a	2.51	8.26	0.50	204.7	5.6	A
18b	2.51	9.08	0.46	85.6	3.1	–
18c	2.51	8.96	0.23	116.4	2.1	A
19	2.49	9.24	0.28	206.0	18.2	–
20	2.57	9.73	1.17	214.1	20.0	–
21	2.54	9.27	0.29	218.8	11.5	A
22	2.51	9.26	0.38	254.6	26.1	A
23	2.52	9.67	0.74	267.3	26.4	A+B
24	2.52	9.33	0.50	375.9	19.4	A+B
25	2.53	9.41	0.75	462.1	34.0	–
26	2.51	8.94	0.38	586.2	36.8	A+B
27	2.50	8.80	1.11	596.5	16.7	A+B
28	2.53	9.25	0.31	764.6	68.1	B
29	2.52	9.27	0.94	765.9	36.5	–
30	2.53	9.08	0.43	886.9	67.4	B

[3]) Fiber densities are calculated from the compositions in table 2 based on a large number of measured values. Their accuracy is ± 0.02 g/cm³.

where M_0 = initial fiber mass in ng, $b = (\bar{d}_0 - 2\,k\,t/\varrho)/(\sqrt{2}\,\sigma)$, $b_0 = \bar{d}_0/(\sqrt{2}\,\sigma)$, $\bar{d}_0$ = average initial fiber diameter in µm, ϱ = fiber density in ng/cm³, σ = standard deviation of the fiber diameter in µm, erf y = error function of y is

$$\operatorname{erf} y = 2/\sqrt{\pi} \int_0^y \exp(-x^2)\,dx.$$

The dissolution-rate constant, k, can be calculated by fitting the fiber weight loss data to equation (2) using non-linear least squares techniques. In section 4. it will be seen that

a) the analysis gives a good fit to the data;

b) the assumptions of the analysis are met for most glass fiber compositions despite a complex dissolution process;

c) the analysis gives dissolution-rate constants that appear to describe the in vivo dissolution process.

For the special case of a uniform fiber diameter, equation (2) reduces to:

$$1 - (M/M_0)^{1/2} = 2\,k\,t/(d_0\,\varrho). \qquad (3)$$

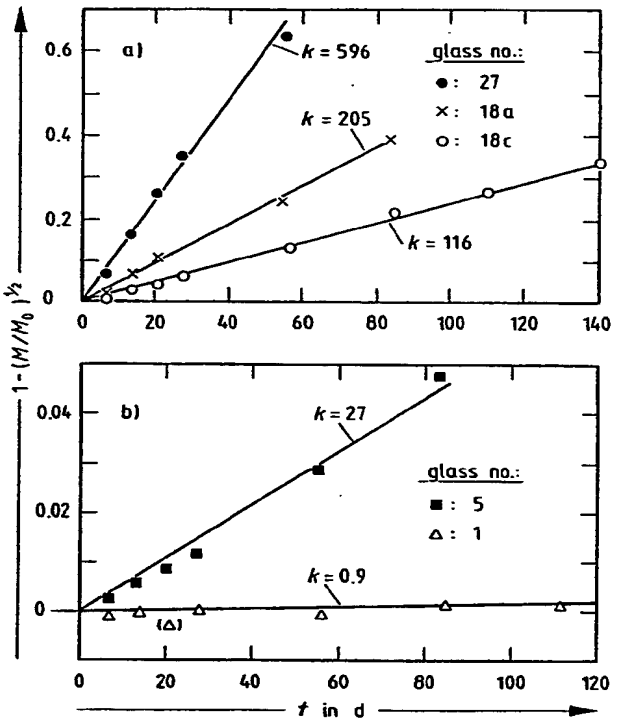

Figures 1a and b. Dissolution data for various glass fibers. The lines are fit to the measured points by equation (2); the corresponding k values are given in ng/(cm² h), a) glasses no. 27, 18a and c, b) glasses no. 5 and 1. The point not used in the fit is enclosed in parantheses.

This is the equation describing dissolution of fibers at a constant dissolution velocity (constant thickness dissolved per time), which follows directly from equation (1) in the case of uniform fiber diameter [3 and 4]. Equation (3) is a close approximation to equation (2) for most of the samples measured here, so that plots of time versus $1 - \sqrt{(M/M_0)}$ are approximately linear. Rate data are plotted in this way in this report but the dissolution-rate constants and the lines through the data have been calculated using equation (2).

4. Dissolution mechanism

Several fiber samples were examined in detail to assure that the method of data analysis is applicable to the dissolution process. The dissolution rates of the glasses no. 1, 5, 18a, c, and 27 span the range of dissolution rates measured (tables 2 and 3). The dissolution data for these glasses are fit well by equation (2) (figures 1a and b), but there is one effect which needs further comment. For each of the five glasses there is an initial period of slower dissolution rate. Scholze and Conradt [4] have noted a similar effect. Whatever the cause, it means that rate constants calculated from only the initial month of dissolution will generally underestimate the rate. For three of the glasses in figures 1a and b the initial rate

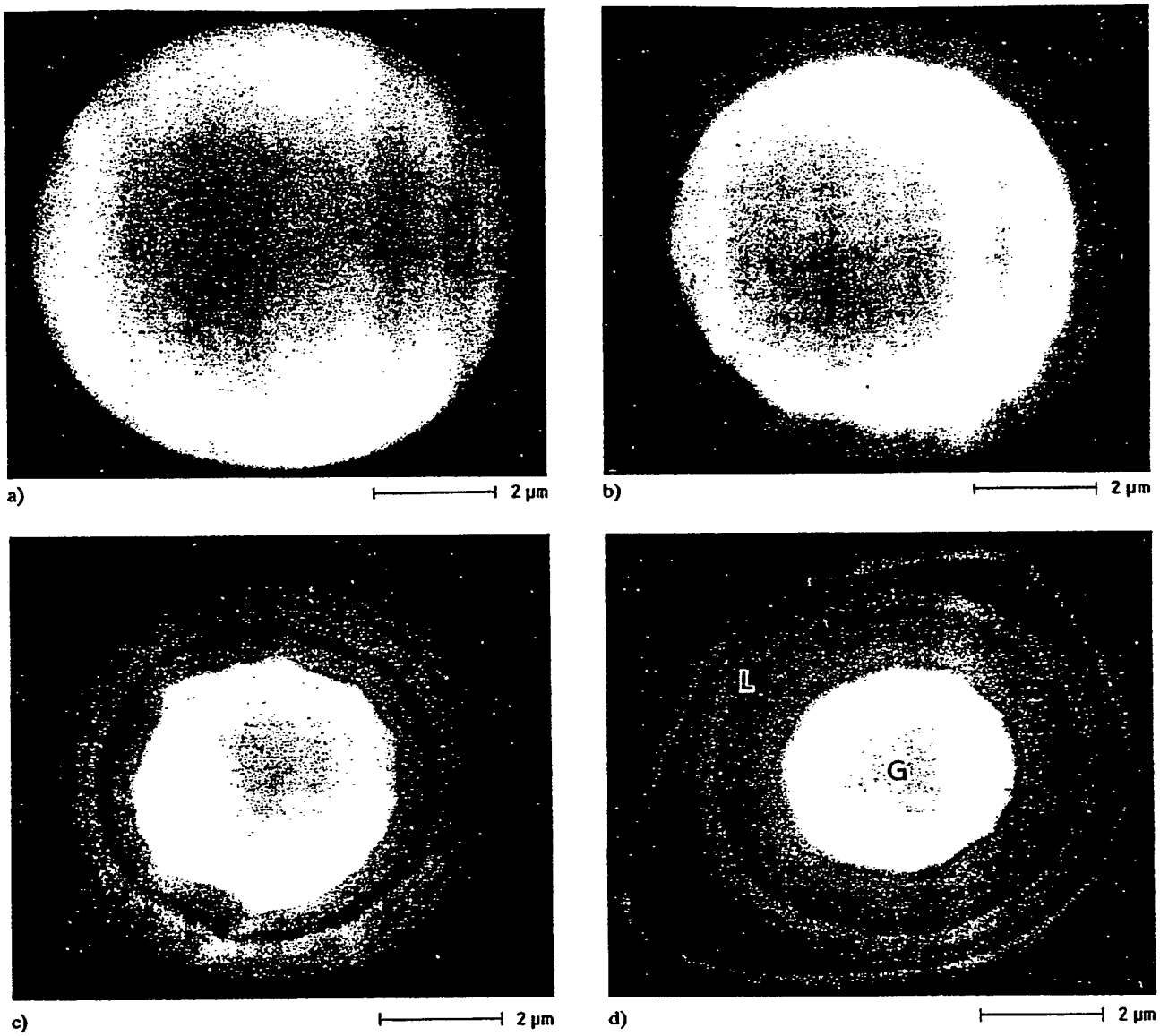

Figures 2a to d. SEM backscattered electron images of glass no. 18a fiber after various dissolution times, t, showing unaltered glass, G, and leached layer, L. Morphology type A, a) untreated, b) $t = 21$ d, c) $t = 55$ d, d) $t = 84$ d.

is the same as that from longer times within the error of the measurement; for two, it is significantly smaller (glass no. 5: 21 %; glass no. 18c: 13 %). The error is not large compared to the variation with glass composition. The dissolution of most glass compositions was therefore followed for only one month. This allowed more compositions to be examined so that a better understanding of the effect of glass composition could be developed.

The partially-dissolved samples of the five glasses were examined under the SEM to correlate weight loss with morphological changes in the fibers. No changes were observed for glasses no. 1 and 5. Apparently the dissolution rates for these glasses are too slow to show morphologic effects within the approximately three-month period of measurement. Samples of glasses no. 18a and c (fiberized from the same glass sample) have the same changes in morphology: a leached layer separated from an unaltered core by a sharp boundary (morphology A, see figures 2a to d). The SEM backscattered electron images, in which brightness is dependent on the density and atomic mass of the material, indicate that the leached layers are lower in density and/or average atomic mass than the core. Energy dispersive x-ray analysis confirms that concentrations of sodium, magnesium, and calcium are much reduced in the leached layer, leaving it enriched in silicon and aluminum. The SEM was unable to resolve finer variations in chemistry. The leached layers are all of approximately uniform thickness around the circumference of any given fiber (fiber no. 2) and there is

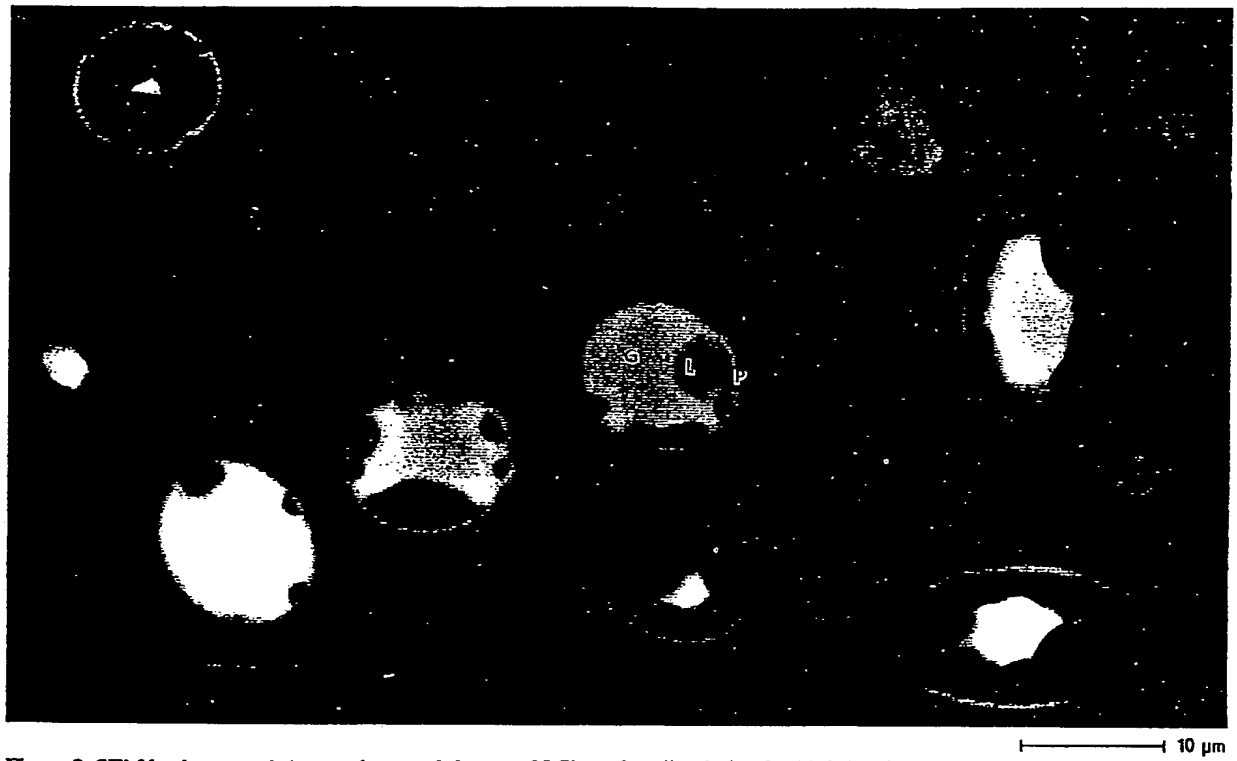

Figure 3. SEM backscattered electron image of glass no. 30 fiber after dissolution for 28 d showing unaltered glass, G, leached layer, L, and protective layer, P, associated with fibers in varying stages of dissolution. Morphology type B.

little variation in thickness of the layers for different fibers in the same sample. This suggests that sample preparation and solution flow rate preclude stagnant areas in the sample. The leached layer thickness increases linearly with time ($r^2 = 0.9989$) while the overall fiber diameter remains essentially unchanged. It appears that the dissolution rate of the leached layer is so slow as to be unmeasurable with the techniques used here. However, one can see in figures 2a to d that the outer layer began to swell (most likely due to hydration) and separate from the fiber. Other SEM pictures show outer layers completely separated; this suggests that the leached layer is mechanically weak and easily removed by physical processes. The rate of increase in leached layer thickness with time of glass no. 18a is 1.8 times greater than that of glass no. 18c. Their dissolution-rate constants determined from weight loss are in the same proportion, indicating that for these two samples, the increase in leached layer thickness is proportional to the rate constant. This large difference in leaching rate between two samples with the same composition is discussed in section 4.2.6. From the data in figures 1a and b and 2a to d and the fiber geometry, the density of the leached layer can be calculated. It is approximately 0.5 g/cm^3, corresponding to a loss of 80 % of its original mass.

Some fibers of glass no. 27 have a dissolution morphology similar to that of glasses no. 18a and c, but others have a different dissolution morphology. This morphology (morphology B) is most clearly illustrated by fibers of a different composition (glass no. 30) which is shown in figure 3. What initially appears to be a bewildering variety of forms, can be understood in terms of a simple set of processes. The initial attack of the solution forms a thin leached layer of the order of 0.5 µm in thickness. This layer protects the fiber from further dissolution so that in some instances the fiber remains unaltered, retaining its original diameter, even after months in solution. More commonly, the layer is breached in places and under the layer rapid dissolution occurs radially into the fiber from these points. Thick leached layers are formed followed by complete dissolution of the fiber material under the outer protective layer. Eventually, the protective layer may disintegrate, leaving a small, leached remnant of the original fiber, which then dissolves completely. Energy dispersive x-ray analysis shows that the leached material is depleted in sodium, calcium, and magnesium. Aluminum is in too low a concentration to be determined. No difference in composition could be found between the protective leached layer and that inside the protective layer. Although the dissolution process seems fairly obvious from the SEM micrographs, the chemical basis for these processes are not yet understood.

The dissolution solutions from those samples kept longest in the fluid were sampled every 2 to 7 d during

Table 4. Major component mass balance for glass no. 18c fiber dissolution after 27.8 d in mg/g initial fiber

	measured		calculated		
	initial fiber	dissolved	dissolved	leached layer	core
SiO_2	620	64	64[5])	49[5])	507
Al_2O_3	39	0	0[5])	7[5])	32
CaO	79	16	14[6])	0[6])	65
MgO	35	6	6[6])	0[6])	29
Na_2O	146	–	27[6])	0[6])	119
K_2O	8	–	1[6])	0[6])	7
B_2O_3	70	14	13[6])	0[6])	57
total	1000	125[4])	125	56	819

[4]) Based on total fiber-weight loss assuming no hydration of leached layer after drying.
[5]) Based on the measured amount dissolved.
[6]) Assuming total removal from the measured leached layer and no removal from the core.

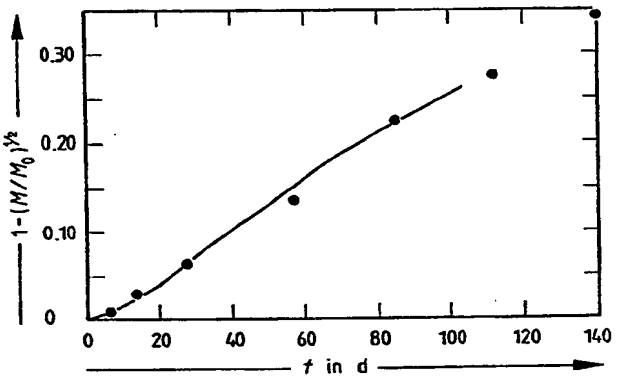

Figure 4. Fiber-weight loss calculated from solution analysis (line) compared to measured weight loss (points) for glass no. 18c fiber.

the dissolution for glasses no. 1, 18c, and 27. The solutions were subsequently analyzed for Al_2O_3, B_2O_3, CaO, MgO, and SiO_2, the major fiber components not originally present in high concentration in the dissolution fluid. It was necessary to correct the CaO and MgO analysis for the amounts originally in the solution. No Al_2O_3 was found in any solution sample.

The solution-analysis data can be combined with weight loss and SEM analyses to give a consistent picture of the dissolution process for several of the glasses. The SEM energy dispersive x-ray analyses suggest that only SiO_2 and Al_2O_3 remain in the leached layers and that SiO_2 is partially leached. For glass no. 18c, the leached layer volume was calculated as a function of dissolution time from the regular dissolution geometry. From the mass of unaltered fiber corresponding to this volume, the concentration of CaO, MgO, and B_2O_3 in the leachate was computed assuming that these oxides were completely removed from the leached layer. To compute

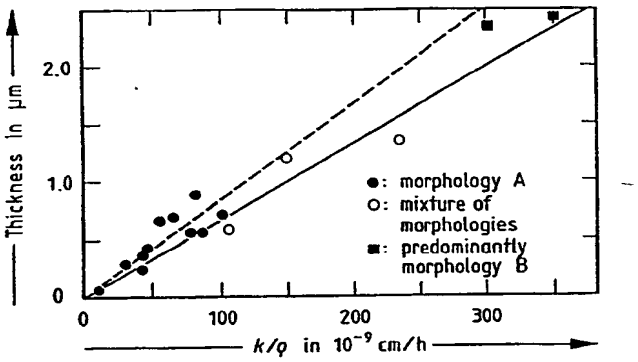

Figure 5. Variation of leached layer thickness at 28 d with dissolution-rate constant calculated by weight loss and normalized by dividing by density. The dashed line shows the theoretical relation based on 80 % weight removal from leached layer, the solid line the calculated reduction in diameter for 100 % removal.

a mass balance it was assumed that Na_2O and K_2O were also completely leached from the leached layer. A comparison of these values for glass no. 18c after dissolution for 27.8 d to the measured values from solution analysis (table 4, the second and third columns, respectively) shows excellent agreement. The sum of the dissolved components is also in agreement with the mass lost from the fiber after 27.8 d and over the entire time during which the solution was monitored (figure 4).

It is not possible to construct tables similar to table 4 for the other two glasses for which the dissolution fluids were analyzed. The leached layer thickness was not measurable for glass no. 1, and glass no. 27 exhibits dissolution morphology B. But plots similar to figure 4 can be constructed for these glasses since the plots do not involve dissolution morphology. The agreement between weight loss and solution-analysis data for glass no. 1 is within the error of the measurements for such a slowly dissolving glass. Weight loss calculated from solution analysis for glass no. 27 is approximately one half of the measured values, indicating some error in the data or the analysis. It is likely that the high solute concentrations resulting from the rapid dissolution of glass no. 27 caused precipitation in the dissolution fluids prior to analysis, but this has not yet been established.

A survey of the dissolution morphologies of selected glasses in tables 2 and 3 was conducted to determine if the results of the detailed studies could be generalized to other fiber compositions. A smooth transition in morphology was found in going from slowly to rapidly dissolving glasses (figure 5). Glasses with slow dissolution rates dissolve with morphology A. As glasses are examined in order of increasing dissolution rate, samples begin to show a few fibers which ar dissolving with morphology B. The number of fibers dissolving with morphology B increases with dissolution rate until it becomes the dominant

morphology for glasses with rapid dissolution rates. In addition to pure morphologies A and/or B, fibers may also exhibit intermediate forms. The factors controlling the shift in morphology from sample to sample and within a given sample are not yet understood and are under investigation.

When the leached layer thickness of a variety of fibers is plotted against dissolution-rate constant calculated from weight loss and normalized by dividing by density (figure 5), fibers with morphology A cluster around a line calculated assuming 80 % weight loss from the leached layer as was found for glasses no. 18a and c. Thus suggests that when morphology A is found, the dissolution process is basically the same regardless of the glass fiber composition. Glasses exhibiting morphology B, where there are some regions of complete dissolution, lie below this line and closer to the line describing the reduction in diameter brought about by complete dissolution.

The mathematical model by which the dissolution-rate constant is extracted from the weight-loss data is based on the assumption that the rate of weight loss is proportional to the reaction-surface area. The work on the dissolution mechanism supports the validity of this assumption for those glass compositions dissolving with morphology A. The theoretical fit to the weight-loss data is good, and the increase in leached layer thickness with time is predicted by the model. This linear dependence eliminates the possibility of control by diffusion across the leached layer. The mathematical model is not completely correct, however, since it assumes complete rather than partial dissolution of the fiber. Equation (2) can be easily modified for the case of firstly, leaching to leave an insoluble layer or secondly, leaching to leave a layer which slowly dissolves (see section 8.). There is uncertainty about which of these modifications, if any, to use for the following reasons:

a) There remains some doubt about the fraction of material remaining in the leached layer and the effect of fiber composition and other variables on this fraction.

b) There have been no measurements of the dissolution rate of the leached layer.

Figure 6 shows the fit of the extreme assumptions — equation (2) assuming 100 % dissolution and equation (9) (section 8.2.) assuming an insoluble fraction. The data and the curves have two basic regions — an early, approximately linear region and an approach to a constant level. The data collected for nearly all samples fall within the linear region where the two equations fit the data equally well. Glass no. 27, which is illustrated, has a large dissolution-rate constant and was followed for a long time. It exhibits both morphologies A and B. The last 4 data points clearly require some insoluble or much

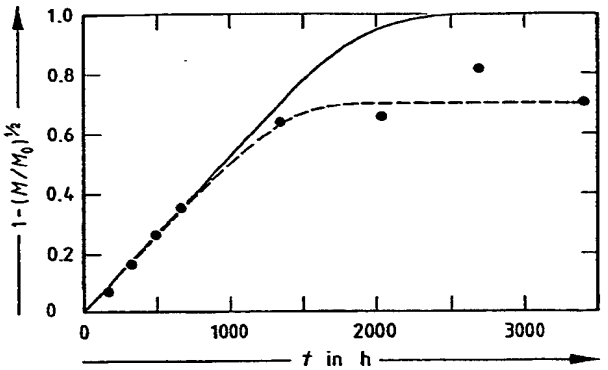

Figure 6. Comparative fits to weight-loss data for glass no. 27. The solid line assumes 100 % dissolution, the dashed line a 9 % insoluble fraction.

more slowly dissolving fraction. The fit to these points is primarily a function of the fraction which is insoluble; the rate constant is the same for both lines. The scatter in these points for this sample may be related to varying proportions of the two morphologies. The insoluble fraction fit to the data is an average of the last four points: 9 %. Glasses leaching with morphology A would be expected to have ≈ 20 % residual material. Glass no. 18c was also followed for long time (figure 1a). It has a rate constant about $\frac{1}{5}$ that of glass no. 27 and leaches with morphology A. Fitting the data to equation (9) (section 8.2.) with 20 % insoluble fraction gave a dissolution-rate constant 5 % greater than from equation (2).

Most samples were not followed long enough to approach a constant level from which an insoluble fraction could be determined, nor is the fit to the available data improved by using a more complicated equation. Because of these factors and the uncertainties already discussed, equation (2) was used to obtain all rate constants presented in this report. The neglect of the leached layer should introduce no more than a 5 % error.

Equation (2) is not expected to describe the dissolution of glass fibers dissolving with morphology B since the changes in surface area with time are not predictable. The fit to the data is good (figure 6), however, and in the absence of a better model, the dissolution-rate constants were calculated by means of equation (2) for these glasses also.

4.1. Comparison to in vivo data

The literature contains many in vivo studies of glass fiber dissolution, but only three which used fibers of initially uniform diameter and measured fiber diameter change with time [11 to 13]. These provide the most accurate measurement of in vivo fiber dissolution rate since they avoid uncertainties associated with a broad fiber diameter distribution. The composition of the fibers used in all three studies is that of

Table 5. Fiber dissolution rate constants for glass no. 5 calculated from literature in vivo data

fiber dimensions diameter × length in μm	animal	fiber location in lung	k in ng/(cm² h)	reference
1.5 × 5	rat	unspecified	1.7	[11]
1.5 × 5	rat	tissue	2.1	[13]
1.5 × 60	rat	unspecified	8.7	[11]
1.5 × 60	rat	tissue	4.1	[13]
1.5 × 60	rat	macrophages	10.4	[13]
3.0 × 10	rat	unspecified	0.0	[11]
3.0 × 60	rat	unspecified	17.4	[11]
3.0 × 10	hamster	unspecified	15.2	[12]
3.0 × 30	hamster	unspecified	48.5	[12]
3.0 × 60	hamster	unspecified	48.2	[12]

in vitro dissolution-rate constant, k, from this study: 27.4 ng/(cm² h)

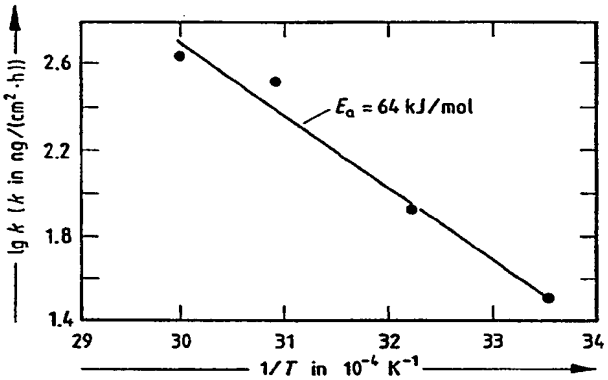

Figure 7. Arrhenius plot for dissolution of glass no. 18b fiber showing the least-squares fit to the data.

glass no. 5. Dissolution-rate constants were calculated from the data in these studies assuming a linear decrease in fiber diameter with time. These calculated dissolution-rate constants appear in table 5 together with other pertinent experimental data from these studies and the in vitro dissolution-rate constant for glass no. 5 measured in this study. The in vivo dissolution rate varies greatly with local environment in the animal and with animal species. The in vitro rate is well within this range. This agreement is not proof that the in vitro rates are good measures of in vivo dissolution rates, but it is comforting that the agreement is as good as the quantity and quality of the data permit. Clearly, in vivo measurements of different compositions are necessary to evaluate fully the accuracy of the in vitro results.

Fibers recovered from animals show a different morphology from those generated in in vitro experiments. There is a reduction in diameter with no evidence of a leached layer. Scholze [5] attributes this to the in vivo presence of organic complexing agents which remove the leached material as it is formed. Alternatively, its mechanical weakness may lead to physical removal while in the animal or during the extraction process. The absence of the leached layer suggests that the leaching process is the rate-determining step in vivo as it is in this study in vitro. The dissolution-rate constants measured in vitro would then underestimate the in vivo rate in ng/(cm² h) by about 30 % in the worst case with 20 % retained in the leached layer.

4.2. Effects of experimental parameters

Some work was devoted to the effects of several of the experimental parameters on the dissolution-rate constant in order to develop a rough feel for their importance. This section summarizes the results.

4.2.1. Solution composition

The physiological saline solution used routinely in this work is only an approximation to what is thought to exist in the lung. The dissolution rates of several samples were measured in two additional fluids to give an indication of the importance of fluid composition. These fluids are human blood plasma and that developed and used by Scholze and Conradt [4] with the addition of 0.1 % NaN_3. The compositions of these fluids and the glass dissolution-rate constants measured in them are summarized in table 5. The data are limited but suggest that fluid composition can change the rate constant by at least a factor of two. In addition, some measurements were made in deionized water (2 glasses) and 0.1 mol [Tris/HCl]/l pH 7.4 buffer (9 glasses). The rate in deionized water is about ¼ that in the modified Kanapilly solution; that in the Tris buffer, about $^1/_{10}$. The dissolution-rate constant for glass no. 18a measured in the Kanapilly solution without the NaN_3 additive was within experimental error the same as that measured in the modified Kanapilly solution.

4.2.2. Temperature

Dissolution rates were measured routinely at 37 °C. Although higher temperatures offer the advantages of increased dissolution rate and reduced bacterial and algal growth, these advantages are outweighed by the uncertainty of extrapolation to body temperature. Also, the physiological saline solutions tend to be less stable toward precipitation at higher temperatures. The effect of temperature was measured in the range 25 to 60 °C for glass no. 18b. The data appear linear in an Arrhenius plot (figure 7), yielding an activation energy of 64 kJ/mol.

4.2.3. Flow rate

For accurate results from a flow-through technique, the solution around the fibers must be exchanged rapidly enough so that the concentration of materials

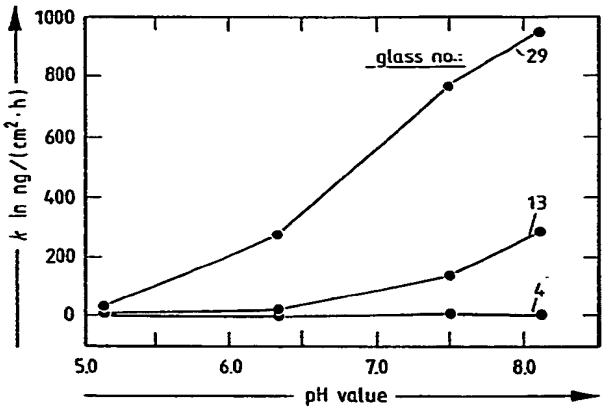

Figure 8. Effect of pH value on dissolution-rate constant, k, for 3 glasses.

Table 6. Comparison of dissolution-rate constants, k, for different fiber diameters of various glasses under different pH conditions

glass no.	pH value	k in ng/(cm² h)		difference in %
		at 10 µm fiber diameter	at 2 µm fiber diameter	
18a	7.5	204.7	260.0	27
13	6.3	24.0	30.7	28
	7.5	139.0	156.0	12
	8.1	285.9	308.6	8
29	6.3	274.8	247.3	10
	7.5	765.9	639.0[7])	17
	8.1	950.1	879.6[7])	7

[7]) Based on only one point.

dissolved from the fibers does not influence the dissolution rate. Large flow rates with uniform bathing of fibers are thus desirable. Balancing this is the need to keep flow rates low to limit consumption of the dissolution fluids. The dissolution rate of glass no. 18a was measured for flow rates in the range 0.08 to 1.00 ml/min. Within this range the dissolution rate is independent of flow rate indicating that these rates are sufficiently rapid to eliminate the effects of dissolved components for these glasses. The standard flow rate of 0.2 ml/min was chosen to be well above the lower limit of this range. The fact that the fluid was generally unchanged in pH value after passing through the sample cells confirm that this is a good choice of flow rate for all but the most rapidly dissolving compositions.

4.2.4. pH value

The dissolution rates of three glass fiber compositions were studied as a function of the pH value in the range 5 to 8. The fiber compositions were chosen to include a rapidly dissolving glass, a slowly dissolving glass, and one in between. The pH value of the fluid was changed with the minimum possible change in the fluid composition. Within limits it was possible to change the pH value of the standard fluid simply by changing the composition of the bubbling gas: 0.5 % CO_2 in air for a pH value near 8 and 50 % CO_2 in air for a pH value near 6. In order to decrease the pH value to near 5, $NaHCO_3$ (routinely 2268 mg/l) was eliminated from the fluid, and it was bubbled with pure CO_2. Glass fiber dissolution rate was found to increase strongly with the pH value (figure 8 and table 6).

4.2.5. Filter-pore diameter

Scholze and Conradt [4] reported that filter-pore diameter strongly affected their rates as measured by silica analysis. In the present experiments, reduction in vacuum-filtration rate after partial dissolution suggested that the filters were generally retaining partially-dissolved fine material, but SEM analysis never showed any build-up of fine material against the filter. Variation in filter-pore diameter from 0.1 to 0.8 µm for glass no. 18b had no effect on the measured dissolution rate.

4.2.6. Fiber diameter and fiber-forming conditions

Glass wool insulation is produced by several manufacturing processes and has a broad distribution of diameters with a mean of ca. 5 µm. Ideally the fiber diameter for dissolution studies should be in the range trapped in the lung, less than 3 µm and have a narrow distribution. It is difficult and time-consuming to form fibers with a uniform diameter this small, and they are difficult to disperse adequately in the sample cells. Therefore, fibers approximately 10 µm in diameter were used routinely. If the assumptions underlying equations (1 and 2) are correct, dissolution-rate constants calculated from equation (2) should be the same regardless of the diameter of the fiber used in the experiment unless differences in forming conditions change fiber properties affecting dissolution rate. For instance, the more rapid quenching rate associated with smaller diameter fibers might lead to a more open glass structure, causing an increase in dissolution rate. To evaluate such effects, several glass compositions were formed into fibers near 2 µm in diameter and the dissolution-rate constants measured. The rates are compared to those from the 10 µm diameter fibers in table 6 for several different pH values. Glasses no. 13 and 18a have consistently higher rates for the 2 µm fibers. The reverse is true for glass no. 29. These differences are within the 95 % confidence limits of the dissolution-rate constants, but the systematic differences seen for each glass type suggest that the differences are real. The dissolution rates of the 2 µm fibers of glass no. 29 are probably anomalously low due to

poor dispersion of the fiber in the sample. Poor dispersion has a greater effect on the more rapidly dissolving glasses, and SEM analysis suggests that this has occurred for the 2 μm fibers of glass no. 29. Further work should be done on the effect of fiber diameter, but for the present purposes, the agreement in dissolution rate for different diameter samples shown in table 6 is sufficient to allow use of 10 μm fibers for routine work.

The various processes used to manufacture glass wool insulation enforce different forming conditions such as quench rate. Although these results on fiber-diameter effects suggest that the fiber-dissolution rate is not strongly influenced by forming conditions, there is some evidence to the contrary. Throughout this study, glasses no. 18a to c were used as standards to measure the effects of various xperimental parameters. Twice the supply of fibers was exhausted, and it was necessary to form more. Thus, there is data on three fiber batches of glass no. 18, all made from the same bulk glass sample. The dissolution rates measured on these samples vary by over a factor of 2 (table 3). This variation reflects differences in the fiber samples rather than in the experimental conditions since several other fiber samples were remeasured occasionally (glasses no. 13, 18a, 29) and their dissolution rates did not change. Chemical analysis of the three glass no. 18 fiber samples showed no difference in composition, so the variation in dissolution rate must reflect differences in the physical state of the fiber. Work is in progress to understand this variation in rate.

5. Effect of glass composition

The results described thus far suggest that the dissolution-rate constants calculated from the dissolution experiments describe the in vitro dissolution of glass fibers with reasonable accuracy up to the point at which the entire fiber has been leached. A significant, unexplained variation in dissolution rate has been found that appears to result from differences in the physical state of the fiber, but this variation is still much less than the variation in rate across the compositional range examined (table 3). The technique thus appears applicable for survey work on a large number of glasses to determine how the in vitro dissolution rate varies with composition.

Tables 2 and 3 list the chemical compositions and dissolution-rate constants of the glasses used in this study in order of increasing dissolution rate. It is clear that chemical composition can have a profound effect on dissolution rate. Glass fibers which have nearly identical shape and size and which have been formed in the same manner, show a variation in dissolution rate of nearly three orders of magnitude. This variation must be ascribed to the compositional variation of the glasses, which is within a fairly narrow range in terms of the possible compositional variation of glass fibers.

Some of the effects of the individual components are obvious from a visual inspection of the tables. The primary compositional effect appears to be that of Al_2O_3, which strongly reduces dissolution rate, as seen by comparing glasses no. 4, 13, and 26. This conclusion supports that of Bauer et al. [6]. In addition, B_2O_3 appears to increase dissolution rate (compare glasses no. 6 and 13), although the influence is not so pronounced as that of Al_2O_3. A more systematic analysis by standard linear least-squares fitting techniques showed the influences of the other oxides. Although some complications arise due to the fact that the dissolution mechanism is gradually changing as the dissolution rate increases, the major oxide components clearly fall into three categories:

first, Al_2O_3: which strongly decreases dissolution rate by a factor approximately two times greater than those of the second group;

second, B_2O_3, BaO, Na_2O, CaO, and MgO: which all increase dissolution rate to about the same degree, although the effect of B_2O_3 is slightly larger;

third, SiO_2: which does not strongly influence the dissolution rate.

Typical glass wool insulation is based on small variations around the composition given by Mohr and Rowe [14]. This compositional range is much narrower than that covered in this study. The dissolution rate of glasses within this narrow range was computed to vary between 50 and 300 ng/(cm^2 h).

As a comparison, the durability of chrysotile asbestos from the Thetford Mine in Quebec (Canada) was measured. This weight-loss data was analyzed using a modification of equation (2) for a single fiber diameter (0.084 μm) estimated from surface-area measurements. The measured rate constant of (0.09 ± 0.05) is in good agreement with 0.05 ng/(cm^2 h) calculated from silica loss in a different modification of Gamble's solution presented by Scholze and Conradt [4]. It is much larger than 0.004 ng/(cm^2 h) – a value calculated from surface measurements by Bauer et al. [6]. All these values are much lower than that measured for glass wool.

To see these glasses and the asbestos from another perspective, one can compute how long it would take a 1 μm fiber to dissolve in simulated lung fluid at 37 °C. For glasses with dissolution constants of 50 and 300 ng/(cm^2 h), the time to total solution would be 83 and 15 d, respectively. In contrast, chrysotile with a dissolution-rate constant of 0.09 ng/(cm^2 h) would require 47 080 d or 129 years to dissolve. These computations assume that the leached silica-alumina remnant observed in some in vitro studies is eliminated in a secondary process. This

assumption is supported by the absence of such a leached layer on fibers collected from lungs of animals or humans.

6. Concluding remarks

This work has examined the influence of chemical composition on the dissolution of glass fibers under conditions approximating those thought to exist in the lung. The dissolution rate of compositions close to commercial glass wool varied by 3 orders of magnitude. Several key effects are apparent:

a) The strongest compositional effect is that of Al_2O_3, which greatly retards dissolution. This is a well-known effect for dissolution in water and in neutral salt solutions [15] and has been indicated by earlier studies of glass fiber in physiological saline solution [6]. Al_2O_3 is essentially insoluble in water solutions at a near neutral pH value, but it has a greater effect than simply failing to dissolve. It somehow retards the leaching process for other fiber components as well.

b) Dissolved alkali-metal cations (excluding lithium) present in near-neutral solution accelerate glass dissolution. This effect has been known for some time [15] and has previously been noted for glass fiber dissolution in saline solution relative to distilled water [3]. The work presented here shows the effect to be even greater when the saline solution is compared to a Tris/HCl buffer, in which the pH value is maintained at 7.4.

c) Dissolution morphology has been observed to change as a function of dissolution rate. Neither the cause nor the mechanism is yet known, but the change in mechanism involves the formation of a protective layer which retards the dissolution of the more rapidly dissolving glasses.

The applicability of these results to glass fiber dissolution in the lung remains uncertain. For the limited data available currently, there is good agreement between the measured dissolution rates in vitro and in vivo, and differences in dissolution morphology can be accounted for plausibly. There is a pressing need for quantitative measurements of in vivo fiber dissolution of a number of different fiber compositions so that it can be determined if large differences in in vitro dissolution rate do indeed correlate to similar differences in in vivo dissolution rate. Such comparisons may support the interpretations of chemical and physical processes that are crucial to understanding dissolution of glass in vivo.

*

The authors gratefully acknowledge the following colleagues, who contributed significantly to this work by means of their experimental and/or critical abilities: P. F. Aubourg, J. A. Davis, T. R. Gilbert, P. A. Tavener, T. L. Gano, and H. Spencer.

7. References

[1] Förster, H.: The behaviour of mineral fibres in physiological solutions. In: Biological effects of man-made mineral fibres. Proc. WHO/IARC Conference, Copenhagen 1982. Vol. 2. Copenhagen: WHO 1984. p. 27–59.

[2] Klingholz, R.; Steinkopf, B.: The reactions of MMMF in a physiological model fluid and in water. In: Biological effects of man-made mineral fibres. Proc. WHO/IARC Conference, Copenhagen 1982. Vol. 2. Copenhagen: WHO 1984. p. 60–86.

[3] Leineweber, J. P.: Solubility of fibres in vitro and in vivo. In: Biological effects of man-made mineral fibres. Proc. WHO/IARC Conference, Copenhagen 1982. Vol. 2. Copenhagen: WHO 1984. p. 87–101.

[4] Scholze, H.; Conradt, R.: An in vitro study of the chemical durability of siliceous fibres. Ann. Occup. Hyg. 31 (1987) no. 4B, p. 683–692.

[5] Scholze, H.: Durability investigations on siliceous man-made mineral fibers – A critical review. Glastech. Ber. 61 (1988) no. 6, p. 161–171.

[6] Bauer, J. F. et al.: Solubility and durability of man-made mineral fibers in physiological fluids. Presented at: TAPPI Non-Wovens Conference, Nashville, OH (USA). 1988.

[7] Kanapilly, G. M.: Alveolar microenvironment and its relationsship to the retention and transport into blood of aerosols deposited in the alveoli. Health Phys. 32 (1977) p. 89–100.

[8] Gamble, J. L.: Chemical anatomy, physiology, and pathology of extracellular fluid. 8th ed. Cambridge, MA: Harvard Univ. Press 1967.

[9] Kanapilly, G. M.; Raabe, O. G.; Goh, C. H. T. et al.: Measurements of in vitro dissolution of aerosol particles for comparison to in vivo dissolution in the lower respiratory tract after inhalation. Health Phys. 24 (1973) p. 497–507.

[10] Ganong, W. F.: Review of medical physiology. 10th ed. Los Altos, CA: Medical Publ. 1981. p. 629.

[11] Morgan, A.; Holmes, A.; Davison, W.: Clearance of sized glass fibres from the rat lung and their solubility in vivo. Ann. Occup. Hyg. 25 (1982) no. 3, p. 317–331.

[12] Holmes, A.; Morgan, A.; Davison, W.: Formation of pseudo-asbestos bodies on sized glass fibers in the hamster lung. Ann. Occup. Hyg. 27 (1983) no. 3, p. 301–313.

[13] Bernstein, D. M.; Drew, R. T.; Schidlovsky, G.: Pathogenicity of MMMF and the contrasts with natural fibres. In: Biological effects of man-made mineral fibres. Proc. WHO/IARC Conference, Copenhagen 1982. Vol. 2. Copenhagen: WHO 1984. p. 169–195.

[14] Mohr, J. G.; Rowe, W. P.: Fiber glass. New York (et al.): Van Nostrand Reinhold 1978. p. 20.

[15] Wiegel, E.: Über die Angreifbarkeit von technischen Natron-Kalk-Gläsern durch Neutralsalzlösungen bei verschiedener Temperatur und verschiedener Wasserstoffionenkonzentration. Glastech. Ber. 42 (1969) no. 7, p. 277–284.

8. Appendix: Mathematical derivations for the calculation of fiber dissolution and weight loss

8.1. General derivation

This appendix contains the derivation of the relation between sample mass and time used to calculate fiber dissolution rate constants in this report (equation (2)). It also contains modifications of this equation for two different dissolution conditions.

If the loss of material from a given fiber is proportional to its surface area, then:

$$-\frac{\partial M}{\partial t} = k A \quad \text{or} \quad -\frac{\partial}{\partial t}\left(\frac{\pi}{4} d^2 \varrho L\right) = k \pi d L . \tag{4}$$

In this and the following equations, k = dissolution-rate constant, M = fiber mass, A = fiber-surface area, d = fiber diameter, ϱ =

fiber density, L = fiber length and t = time. When the term in parentheses is differentiated, neglecting the change of length with time, equation (4) reduces to:

$$\frac{\partial d}{\partial t} = -\frac{2k}{\varrho} \tag{5}$$

which can be integrated to yield:

$$d = d_0 - 2k\,t/\varrho \tag{6}$$

where d_0 = initial fiber diameter. This equation can be applied to all fibers.

The initial diameter of the fibers is assumed to follow a Gaussian distribution of mean d_0 and standard deviation σ. If the total number of fibers is N, the probability of having a fiber of diameter d_0 is

$$f(d_0) = \frac{N}{\alpha\,\sigma\sqrt{2\pi}} \exp\left(-\tfrac{1}{2}((d_0 - \bar{d}_0)/\sigma)^2\right).$$

A mormalizing factor α has been introduced to take into account the fact that only positive values of d_0 are being considered:

$$\alpha = \frac{1}{\sigma\sqrt{2\pi}} \int_0^\infty \exp\left(-\tfrac{1}{2}((d_0 - \bar{d}_0)/\sigma)^2\right) \partial d_0 .$$

The mass of a single fiber is $\pi\,d^2\,\varrho\,L/4$. Substituting for d from equation (6) gives:

$$\frac{\pi}{4}\left(d_0 - \frac{2k\,t}{\varrho}\right)^2 \varrho\,L .$$

The total mass of the sample at time t is obtained by integrating over all diameters for $d > 0$. From equation (6), this occurs for $d_0 > 2k\,t/\varrho$. Assuming that all fibers have the same length L:

$$M = \frac{\pi\,\varrho\,L}{4} \frac{N}{\alpha\,\sigma\sqrt{2\pi}} \int_{2k\,t/\varrho}^\infty \left(d_0 - \frac{2k\,t}{\varrho}\right)^2 \exp\left(-\tfrac{1}{2}((d_0 - \bar{d}_0)/\sigma)^2\right) \partial d_0 . \tag{7}$$

Using the notation
$Q(b) = b\,e^{-b^2} + (\sqrt{\pi}/2)\,(1 + 2b)\,(1 + \mathrm{erf}\,b)$.
For the fast dissolving fraction, the mass M_1 varies as:
$M_1/((1-\beta)\,M_0) = Q(b_1)/Q(b_0)$

where $b_1 = [\bar{d}_0 - 2k_1\,t/(\varrho\,(1-\beta))]/(\sqrt{2}\,\sigma)$. (10)

For the slow dissolving fraction, the mass M_2 varies as:

$M_2/(\beta\,M_0) = Q(b_2)/Q(b_0)$

where $b_2 = [\bar{d}_0 - 2k_2\,t/(\varrho\,(1-\beta))]/(\sqrt{2}\,\sigma)$. (11)

The overall equation is

$$\frac{M}{M_0} = \frac{1}{Q(b_0)}\left[(1-\beta)\,Q(b_1) + \beta\,Q(b_2)\right] \tag{12}$$

After integration and simplification, equation (7) becomes:

$$\frac{M}{M_0} = \frac{b\exp(-b^2) + (\sqrt{\pi}/2)\,(1+2b^2)\,(1+\mathrm{erf}\,b)}{b_0\exp(-b_0^2) + (\sqrt{\pi}/2)\,(1+2b_0^2)\,(1+\mathrm{erf}\,b_0)} \tag{8}$$

which is equation (2) in section 3. with

$b = (\bar{d}_0 - 2k\,t/\varrho)/(\sqrt{2}\,\sigma)$; $b_0 = \bar{d}_0/(\sqrt{2}\,\sigma)$ and

$$\mathrm{erf}\,y = \frac{2}{\sqrt{\pi}} \int_0^y \exp(-x^2)\,dx .$$

8.2. Calculation of fiber weight loss curve for an incomplete dissolution

In practice, for type A morphology, the fibers do not dissolve completely but a very porous structure containing alumina and silica remains. This structure dissolves very slowly. After complete leaching, a fraction β of the initial mass M_0 remains. The computation of the change in mass of the fiber with time can be simply treated by considering that the mass of the fiber is the sum of an insoluble part, $\beta\,M_0$, that remains constant with time and a soluble part, $(1-\beta)\,M_0$, that dissolves according to equation (8). In this case, equation (8) becomes:

$$\frac{M - \beta\,M_0}{(1-\beta)\,M_0} = \frac{b'\exp(-b'^2) + (\sqrt{\pi}/2)\,(1+2b'^2)\,(1+\mathrm{erf}\,b')}{b_0\exp(-b_0^2) + (\sqrt{\pi}/2)\,(1+2b_0^2)\,(1+\mathrm{erf}\,b_0)} \tag{9}$$

where

$b' = [\bar{d}_0 - 2k\,t/(\varrho\,(1-\beta))]/(\sqrt{2}\,\sigma)$.

In the following case, the leached layer described in section 3. is assumed to dissolve slowly. The fiber can be considered to consist of a rapidly dissolving fraction of initial mass $(1-\beta)\,M_0$, density $(1-\beta)\,\varrho$, dissolving at rate k_1 and a slowly dissolving fraction of initial mass $\beta\,M_0$, density $\beta\,\varrho$, dissolving at rate k_2. For each fraction, equation (8) applies.

where the total mass $M = M_1 + M_2$. k_1 can be computed at short times, k_2 at long times.

8.3. Derivation for the case of narrow fiber-diameter distribution

If $\sigma \to 0$, $b \to \infty$ (unless $t = \varrho\,d_0/(2k)$) and equation (8) simplifies to

$$M/M_0 \approx (b/b_0)^2 . \tag{13}$$

Substituting the definitions of b and b_0 from equation (8) into equation (13), and recognizing that $\bar{d}_0 = d_0$:

$$(M/M_0)^{1/2} = 1 - 2k\,t/(d_0\,\varrho) \tag{14}$$

which is equation (3) in section 3. 91R0002